2D Materials

LETTER

Low tension graphene drums for electromechanical pressure sensing

Raj N Patel[1,2,3], John P Mathew[1,3], Abhinandan Borah[1] and Mandar M Deshmukh[1]

[1] Department of Condensed Matter Physics and Materials Science, Tata Institute of Fundamental Research, Homi Bhabha Road, Mumbai 400005, India
[2] Physics Department, Birla Institute of Technology and Science Pilani — K. K. Birla Goa Campus, Goa 403726, India
[3] R N P and J P M contributed equally.

E-mail: deshmukh@tifr.res.in

RECEIVED
6 October 2015

REVISED
9 December 2015

ACCEPTED FOR PUBLICATION
16 December 2015

PUBLISHED
18 January 2016

Keywords: graphene, drum resonator, pressure sensor

Supplementary material for this article is available online

Abstract

We present a process to fabricate electromechanical pressure sensors using multilayer graphene in a sealed drum geometry. The drum resonators are fabricated on insulating sapphire substrates with a local back gate for direct radio frequency (rf) actuation and detection of the mechanical modes. Using this scheme, we show the detection and electrostatic tuning of multiple resonant modes of the membrane up to 200 MHz. The geometry of the device also helps in attaining low tensile stress in the membrane, thereby giving high gate tunability (~1 MHz/V) of the resonator modes. We study the resonant frequency shifts in the presence of helium gas and demonstrate a sensing capability of 1 Torr pressure in a cryogenic environment.

1. Introduction

Nanoelectromechanical systems (NEMS) using two-dimensional (2D) materials [1, 2] are potential candidates for use in high-resolution sensors while providing a suitable platform for studies of fundamental physics [3, 4]. Graphene is a prime material for use in such NEMS devices due to its good electrical response, mechanical strength, and sensitivity to external stimuli [5, 6]. For a typical length of 2–4 μm the resonant frequencies of suspended graphene resonator devices are in the 10–100 MHz regime. Direct electrical readout of the mechanical resonance at these frequencies can be challenging due to parasitic capacitance in nanoscale devices. Many NEMS devices based on electrical actuation and detection schemes make use of downmixing techniques to circumvent the signal detection issues in the radio frequency (rf) regime. The clamping conditions of the membrane also play a vital role in the observed mechanical response; a doubly clamped structure could exhibit effects of edge eigenmodes that affect the tunability [7]. Here, we present a fabrication process to build drum resonators of 2D materials on a sapphire substrate to reduce parasitic capacitance and demonstrate electromechanical measurements using a direct capacitive readout up to 200 MHz. We also demonstrate the use of such a device in sensing pressure by studying the frequency shifts obtained in the resonator upon introduction of gas molecules.

Highly resistive sapphire (resistivity $>10^{14}$ Ωm) substrates were used in our devices to eliminate parasitic capacitance. The use of substrates such as intrinsic silicon (resistivity $>10^{6}$ Ωm) is an alternative [8]; however, the finite conductivity of these substrates at room temperature gives rise to parasitics that degrade the rf signals. By using sapphire substrates, rf measurements can be carried out at room temperature [9]. Also, our fabrication process ensures that the flake does not come in contact with any chemicals used in the lithography process. This is achieved by using a dry transfer technique [10] to place the exfoliated flakes at the last stage of fabrication. The free suspension of the flake results in reduced tensile stress, which in turn increases the sensitivity of the device to tension applied by electrostatics or ambient pressure.

2. Fabrication

Figure 1 shows a schematic of the fabrication steps for the multilayer graphene drum resonators on a sapphire (C-plane) substrate. To avoid charging effects of the

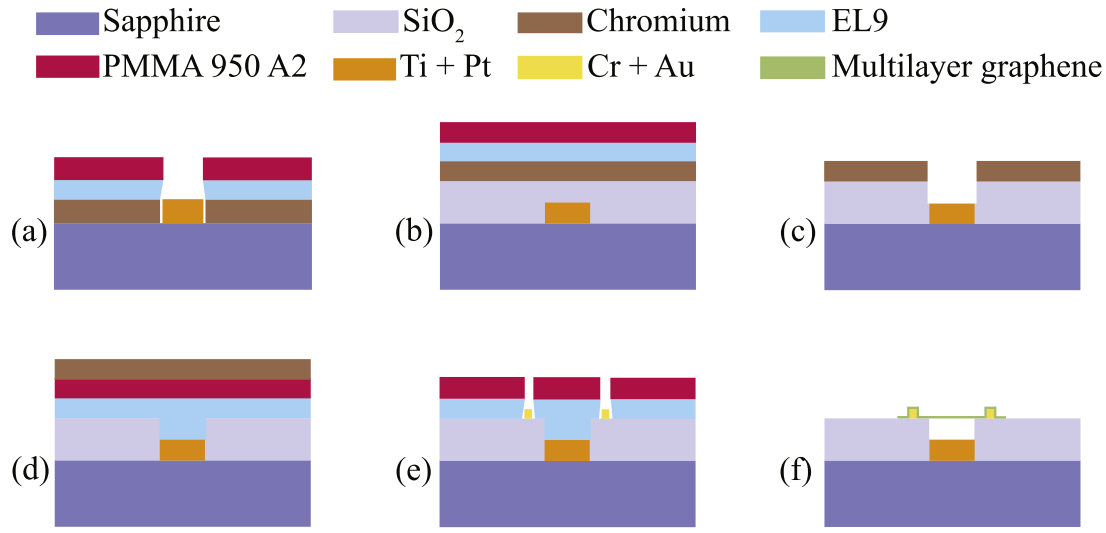

Figure 1. Steps used in the fabrication of a suspended multilayer graphene drum resonator on a hole over a local gate on a sapphire substrate. (a) Patterning of local gate and metal deposition by e-beam evaporation of Ti/Pt (15/10 nm). (b) Deposition of SiO_2 and e-beam lithography to pattern the hole over the local back gate. (c) Developing of resists, etching of Cr, washing off resists, and RIE to etch a hole. (d) E-beam lithography to pattern source-drain electrodes. (e) Etching Cr, developing resists, and thermal evaporation of Cr/Au (10/50 nm) to form source-drain electrodes. (f) Washing off resists with acetone and dry transfer of multilayer graphene over the hole and electrodes.

insulating substrate during e-beam lithography, a thin chromium (Cr) layer (20 nm) is thermally evaporated. Cr is chosen as the conducting layer, because the Cr etchant (Sigma Aldrich 651826) used to etch the metal layer does not affect any other materials such as the substrate, dielectric, and electrode metals that are integrated in the device at different stages. After evaporating the conducting layer of Cr, standard e-beam lithography techniques are used to pattern the local gate (3x3 μm^2). After the removal of Cr from the developed regions of the resists, titanium/platinum (15/10 nm) is deposited as the gate metal using e-beam evaporation (figure 1(a)), followed by lift-off in acetone. The use of the Ti/Pt combination (as opposed to Cr/Au) does not lead to back sputtering when exposed to reactive ion etching later in the process.

After etching the remaining Cr (figure 1(b)), the entire substrate and the local back gate are covered by 300 nm of silicon dioxide (SiO_2) grown by plasma-enhanced chemical vapor deposition at 150 °C. Now the SiO_2 covering the gate region has to be locally etched. An additional region near the outer pad also has to be etched for final wirebonding. For this, Cr is thermally evaporated, resist layers are spin-coated, and e-beam lithography is done to pattern the desired regions of the SiO_2 that have to be etched.

Subsequently the resist layers are developed, and Cr is etched from the developed regions. Due to the micro-scale size of the feature to be wet etched, there is the possibility that the etching does not take place uniformly. To eliminate this problem, the Cr etchant is stirred using a magnetic stirrer. The substrate is dipped in the etchant for 60-90 s and then rinsed in deionized (DI) water and subsequently in isopropyl alcohol. The resist layers are then removed using acetone to prevent hard baking. Reactive ion etching (RIE) is used to dry etch SiO_2 in the desired region (figure 1(c)). The un-etched Cr protects the surrounding SiO_2 from getting etched. After RIE, the remaining Cr is removed using the wet etchant.

In the next step, source-drain electrodes are designed near the hole. For this, resist layers are spin-coated, and a 20 nm Cr layer is thermally evaporated on the resist. E-beam lithography is done to pattern the electrodes. The resist layers are developed after etching the top Cr layer. As seen in figure 1(e), thermal evaporation of chromium (10 nm) and gold (50 nm) is performed to form source-drain electrodes, followed by lift-off in acetone.

Finally, multilayer graphene is mechanically exfoliated on a PDMS (polydimethylsiloxane) film. Flakes are located using an optical microscope [11, 12]. The selected flake is then transferred using a dry transfer technique [10] on the device (figure 1(f)) such that it covers the hole and the source-drain electrodes. The thickness of the multilayer graphene flake used in device 1 is ~7.5 nm, corresponding to 21 layers.

3. Resonance measurements

Figure 2(a) shows a three-dimensional (3D) schematic of the final device. The source, drain, and gate electrodes are wirebonded onto a chip carrier for further measurements. Before performing any electrical measurements, scanning electron microscope (SEM) imaging of the membrane is done to ensure it is free of cracks and wrinkles. Figure 2(b) shows the SEM image of a multilayer graphene drum device. SEM

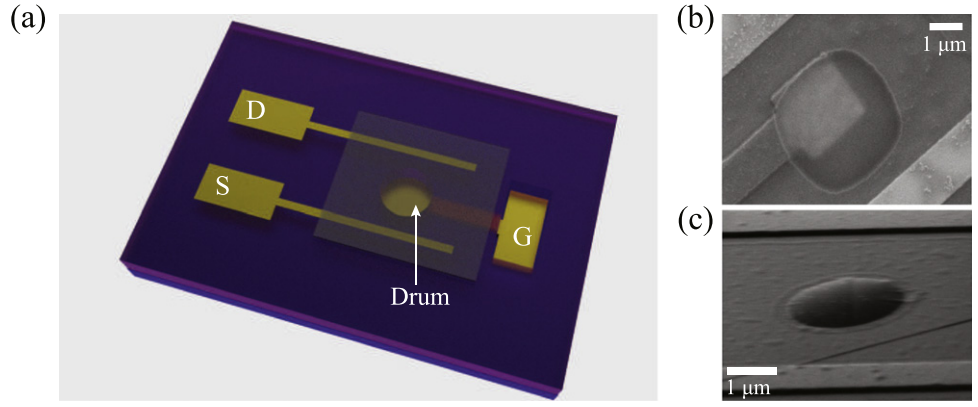

Figure 2. (a) A 3D schematic of final device. The electrode below the two holes represents the local back gate. Multilayer graphene is transferred over the smaller hole and the source-drain electrodes. The bigger hole allows wirebonding of the local back gate. (b) SEM image of a drum resonator just after the transfer step. (The SEM images were taken following the precautionary steps described in section A of the supporting information.) (c) SEM image of a bulged multilayer graphene flake.

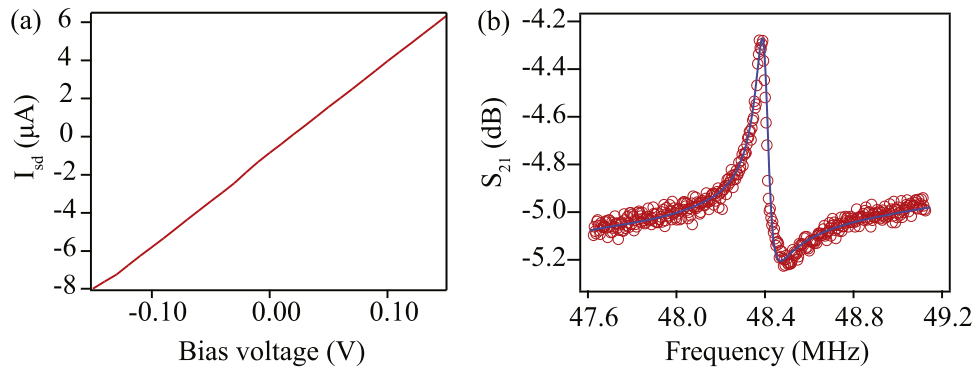

Figure 3. (a) IV response of device 2 measured at 5 K with −19 V gate voltage. This includes the constant line resistance of 20 kΩ of the circuit used, which is subtracted to get the actual resistance of the device. (b) S_{21} response of device 2 taken at 5 K, $V_{sd}^{dc} = 0$ V, −19 V gate voltage, and -44 dBm drive power. The blue line is the fitted response, giving a quality factor of 773.

imaging of the flake is important to confirm that it is intact and suspended. An important precaution to be taken while imaging suspended drum devices fabricated on sapphire substrates is to ground the gate and source-drain electrodes; electrical charges that accumulate on the membrane can lead to rupturing in the absence of electrical grounding. The device is then loaded in a vacuum chamber and pumped for 3 days to remove gas trapped below the membrane; this pumping takes long time due to the impermeability of graphene to any gas, as reported by Bunch *et al* [13]. Figure 2(c) presents an SEM image of the drum, which was pumped for a few hours and imaged. The bulging of the suspended portion of the flake indicates the presence of gas that has not been pumped out completely, giving rise to a higher pressure inside the hole compared to the vacuum in the SEM chamber.

The samples are initially measured in a vacuum can at room temperature and then in a 4 He cryostat at 5 K. Room temperature data is included in the supporting information. Figure 3(a) shows the measured IV response of the device at 5 K. The resistance of the device is approximately 1.5 kΩ. Figure 3(b) shows the measured transmission coefficient S_{21} taken at 5 K for zero applied bias, $V_g = -19$ V, and −44 dBm drive power. The quality factor is extracted from fitting the response, giving a $Q \sim 773$.

The circuit [14] used to actuate and detect mechanical motion in the drum resonators is shown in figure 4(a). An rf signal supplied from a network analyzer (Agilent 4396B) is combined with a dc voltage, V_g, using a bias tee and applied to the local back gate. A dc bias, V_{sd}^{dc}, is applied to the source electrode. The drain current is separated into rf and dc components using a bias tee. The rf signal is amplified by an amplifier fixed on the cryostat insert and then further by a low-noise preamplifier (SRS-SR445A) before being fed to a network analyzer. The rf current through the resonator is then given by [14]

$$\tilde{I} = j\omega C_{tot}\tilde{V}_g - j\omega\frac{\tilde{z}}{z_0}C_g V_g + V_{sd}^{dc}\frac{dG}{dV_g}\tilde{V}_g - V_{sd}^{dc}\frac{dG}{dV_g}\frac{\tilde{z}}{z_0}V_g \quad (1)$$

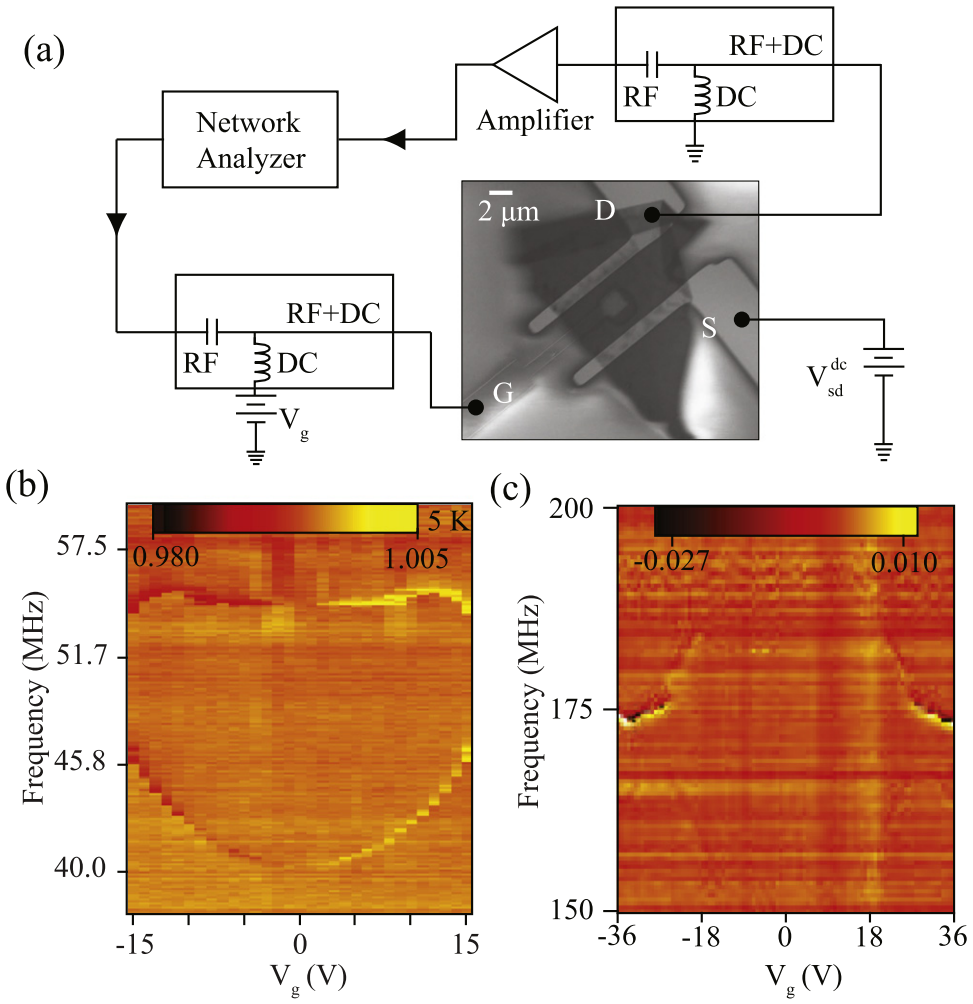

Figure 4. (a) Schematic of the circuit used for actuation and detection of mechanical resonance in the multilayer graphene device. (b) Measured resonance response of device 1 as a function of V_g at $V_{sd}^{dc} = -300$ mV and -10 dBm drive power (response in dB). (c) Frequency response with gate voltage in the frequency range 150–200 MHz for device 2 at $V_{sd}^{dc} = 0$ V at 300 K (background subtracted, response in dB).

where ω is the drive frequency, C_{tot} is the total capacitance between gate and drain, $\tilde{V}_g$ is the amplitude of the rf drive, $\tilde{z}$ is the amplitude of vibration of the membrane, z_0 is the distance of the membrane from the gate, V_g is the applied gate voltage, and $\frac{dG}{dV_g}$ is the transconductance. In presence of a dc bias, V_{sd}^{dc}, the third and fourth terms in (1) contribute significantly due to the gate modulation of conductance. However, the sensitivity of this technique allows us to measure the response of the resonator even at $V_{sd}^{dc} = 0$ V. For zero source-drain voltage, we are probing the mechanical motion of the membrane purely due to the modulated distance of the gate-membrane capacitor system (as seen from the second term in (1)). This implies that we can carry out electromechanical measurements of materials having zero transconductance.

Figures 4(b) and (c) show the resonant frequency as a function of the applied dc gate voltage, V_g. Multiple resonant modes are observed with increasing frequency up to 200 MHz (additional data in section B of supporting information). The fundamental mode (~40 MHz) of the membrane is seen to have a good tunability with the gate voltage. As the initial tension in the membrane is low, the electrostatic pull by the gate contributes an additional tension that monotonically increases the resonance frequency with the magnitude of the gate voltage. We see that the resonance frequency tuning is ~1 MHz/V. The good electrostatic control of the drum frequency allows for further studies of parametric amplification and instabilities in similar systems. The low tension state of the drum as reflected in the large frequency tuning is critical for the experiments we describe next.

4. Pressure sensing

To demonstrate the potential of these devices, we performed experiments that exploit the dependence of the resonator mode frequency on the force exerted by gas molecules above the membrane. We studied the effect of pressure on top of the membrane surface by introducing a known quantity of helium gas. These

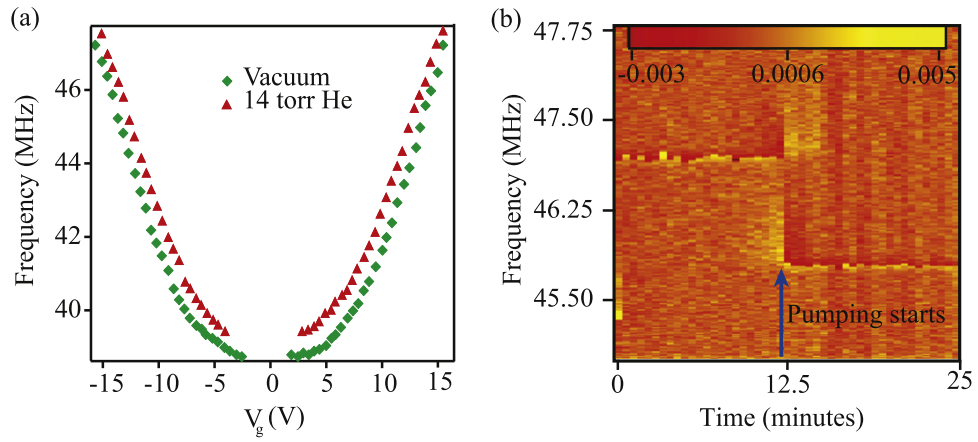

Figure 5. (a) Measured resonance response of device 1 as a function of V_g at $V_{sd}^{dc} = -300$ mV and −10 dBm drive power in the presence of helium (red) and in vacuum (green) at 70 K. (b) Change in resonance frequency measured with time (t') in the presence of helium with pressure 14 Torr (from t′ = 0–12 min) and in vacuum after t'=12 min (background subtracted, response in dB).

measurements were carried out at 70 K, where the reference gas pressure was measured using a Baratron gauge (MKS) placed at the mouth of the cryostat at room temperature. Figure 5(a) shows the response of the first mode frequency with the gate voltage in vacuum and in the presence of 14 Torr of helium gas for device 1. In both cases the resonance frequency increases monotonically with increasing magnitude of the gate voltage. This monotonicity, as mentioned earlier, is an indication that the behavior of the mode is entirely dominated by the tension produced by the attractive electrostatic force towards the gate [15]. The gas aids the capacitive pull by the gate, thus increasing the tension and resonant frequency of the drum at a given gate voltage. Additionally, the response of the mode at a fixed gate voltage was monitored in time when the gas molecules were again pumped out. Figure 5(b) shows the resonance frequency shift upon removal of the helium. The system was pumped out at the 12 minute mark, at which point the resonance frequency drops from ~47 to 46 MHz. The timescale in which the experiments were performed was small enough not to allow diffusion of helium molecules into the drum at low temperatures [13]. From the change in resonance frequency between two states (in vacuum and with gas), we can calculate the pressure change in the system.

The membrane has zero flexural rigidity and is under a small initial strain, Γ_0, with an initial parabolic deflection, z_0, towards the gate. We model our system as a mass, m_{eff}, attached to a spring of stiffness k, where the stiffness is decided by the initial tension in the membrane and the gate voltage-induced displacement. The tension in the membrane depends on the mode shape and is balanced by the electrostatic attraction to the gate electrode. The presence of gas above the membrane modifies the stiffness in the system by shifting the equilibrium position of the membrane closer to the gate electrode. We calculated the contribution of pressure, P, to the total energy of the electromechanical system and found the new effective spring constant, k_{eff}, in the presence of gas, where $k_{eff} = k_{eff}(V_g, P)$ (see section C of supporting information for detailed analysis) [16]. Initial strain, z_0, and effective mass were used as parameters to fit the experimentally observed frequency response with the gate voltage in vacuum. This effective mass can be different from the actual mass of the membrane due to residue from fabrication and adsorption of gas molecules and can be mode-shape dependent [5, 15, 16]. The fitting parameters were found to be $z_0 = 6$ nm, $\Gamma_0 = 0.03\%$, and m_{eff} as 2.2 times the actual mass of the membrane. The value obtained for strain is lower than in similar systems and shows that our device is under low tension [8]. Subsequently, P was used as the only free parameter to fit the frequency response with the gate voltage in the presence of gas. The value of P obtained from fitting was 15.7 Torr, in close agreement to the reference value measured by an independent gauge. As a frequency shift of 1 MHz is observed for gas pressure of 14 Torr, and as the quality factor of these devices is near 500, this translates to a pressure sensing resolution of 1 Torr in these devices.

5. Conclusion

In conclusion, we have developed a fabrication process for low-tension electromechanical drum resonators using multilayer graphene membranes. The scheme ensures that the cleanliness of the exfoliated material is not affected by the chemicals involved in the process at any stage. The use of a sapphire substrate enables easy and direct readout of high-frequency signals up to 200 MHz. These drum devices also find application as pressure sensors with a resolution of 1 Torr at cryogenic temperatures. They are analogous to the resonant silicon diaphragm sensors [17], and with

improvements in design and quality factors, the sensitivity of these devices can be improved so that they can detect pressures ~0.1 Torr. These sensors, because of their small dimensions, can be integrated in an array of microfabricated chambers for cryogenic experiments.

Acknowledgments

We acknowledge the Department of Atomic Energy, Government of India for financial support. We thank Dr Abhilash T S for discussions. We would like to acknowledge Bhagyashree Chalke, Rudheer Bapat, Amit Shah, and Gajendra Mulay for technical support. We also thank Sameer Grover for help with the figures.

References

[1] Jaesung L, Zenghui W, Keliang H, Jie S and Philip X-L F 2013 High-frequency MoS_2 nanomechanical resonators *ACS Nano* **7** 6086–91
[2] Castellanos-Gomez A, van Leeuwen R, Buscema M, SJ H, van der Zant G A, Steele and Venstra W J 2013 Single-layer MoS_2 mechanical resonators *Adv. Mater.* **25** 6719–23
[3] Koenig S P, Boddeti N G, Dunn M L and Bunch J S 2011 Ultrastrong adhesion of graphene membranes *Nat. Nanotechnol* **6** 543–6
[4] Singh V, Bosman S J, Schneider B H, Blanter Y M, Castellanos-Gomez A and Steele G A 2014 Optomechanical coupling between a multilayer graphene mechanical resonator and a superconducting microwave cavity *Nat. Nanotechnol* **9** 820–4
[5] Bunch J S, van der Zande A M, Verbridge S S, Frank I W, Tanenbaum D M, Parpia J M, Craighead H G and McEuen P L 2007 Electromechanical resonators from graphene sheets *Science* **315** 490–3 January
[6] Koenig S P, Wang L, Pellegrino J and Bunch J S 2012 Selective molecular sieving through porous graphene *Nat. Nanotechnol* **7** 728–32
[7] Garcia-Sanchez D, van der Zande A M, Paulo A S, Lassagne B, McEuen P L and Bachtold A 2008 Imaging mechanical vibrations in suspended graphene sheets *Nano Lett.* **8** 1399–403
[8] Sunwoo L *et al* 2013 Electrically integrated SU-8 clamped graphene drum resonators for strain engineering *Appl. Phys. Lett.* **102** 153101
[9] Abhilash T S, Mathew J P, Sengupta S, Gokhale M R, Bhattacharya A and Deshmukh M M 2012 Wide bandwidth nanowire electromechanics on insulating substrates at room temperature *Nano Lett.* **12** 6432–5
[10] Castellanos-Gomez A, Buscema M, Molenaar R, Singh V, Janssen L, van der Zant H S J and Steele G A 2014 Deterministic transfer of two-dimensional materials by all-dry viscoelastic stamping *2D Mater* **1** 011002
[11] Blake P, Hill E W, Neto A H C, Novoselov K S, Jiang D, Yang R, Booth T J and Geim A K 2007 Making graphene visible *Appl. Phys. Lett.* **91** 063124
[12] Hai L, Jumiati W, Xiao H, Gang L, Jian Y, Xin L, Qihua X and Hua Z 2013 Rapid and reliable thickness identification of two-dimensional nanosheets using optical microscopy *ACS Nano* **7** 10344–53
[13] Bunch J S, Verbridge S S, Alden J S, van der Zande A M, Parpia J M, Craighead H G and McEuen P L 2008 Impermeable atomic membranes from graphene sheets *Nano Lett.* **8** 2458–62
[14] Xu Y, Chen C, Deshpande V V, DiRenno F A, Gondarenko A, Heinz D B, Liu S, Kim P and Hone J 2010 Radio frequency electrical transduction of graphene mechanical resonators *Appl. Phys. Lett.* **97** 243111
[15] Singh V, Sengupta S, Solanki H S, Dhall R, Allain A, Dhara S, Pant P and Deshmukh M M 2010 Probing thermal expansion of graphene and modal dispersion at low-temperature using graphene nanoelectromechanical systems resonators *Nanotechnology* **21** 165204
[16] Changyao C 2013 Graphene Nanoelectromechanical Resonators and Oscillators *PhD Thesis* Columbia University
[17] Stemme G 1991 Resonant silicon sensors *J. Micromech. Microeng* **1** 113–25 June